Effects of Volume Diffusion in Heat Transfer in a Cavity Flow in Non-Continuum Regime

Chariton Christou[a] and S Kokou Dadzie[b]

School of Engineering and Physical Sciences, Heriot-Watt University, Edinburgh, EH14 4AS, Scotland, UK

[a)]Corresponding authors: c.christou@hw.ac.uk
[b)]k.dadzie@hw.ac.uk

Abstract. Volume diffusion (or bi-velocity) continuum model offers an alternative modification to the standard Navier-Stokes-Fourier for simulating rarefied gas flows. According to this continuum model, at higher Knudsen numbers the contribution of molecular spatial stochasticity increases. In this paper, we study a micro-cavity heat transfer problem as it provides an excellent test for new continuum flow equations. Simulations are carried out for Knudsen numbers within the slip and higher transition flow regimes where non-local-equilibrium and rarefaction effects dominate. We contrast predictions by a Navier-Stokes-Fourier model corrected by volume diffusion flux in its constitutive equations to that of the Direct Simulation Monte Carlo method and the standard Navier-Stokes-Fourier model. The results show improvement in the Navier-Stokes-Fourier prediction for the high Knudsen numbers. The new model exhibits proper Knudsen boundary layers in the temperature and velocity fields.

INTRODUCTION

The use of micro- and nano- electromechanical systems (MEMS/NEMS) has faced rapid increase as it has generated extensive research in fluid flows in ultra-small devices. Gas flows at micro- and nano-scale involve complex processes due to rarefaction, important gas-surface interactions, and inter-molecular collisions[1]. Classical continuum fluid equation models like the standard Navier-Stokes-Fourier (NSF) fail to describe flows under these conditions[1]. The degree of gas rarefaction can be determined by the Knudsen number (Kn), Kn = λ/L, which can be defined as the ratio of the gas molecular mean free path (λ) to the characteristic length scale of the flow system (L)[2].

In order to describe micro- and nano-scale flows, the Boltzmann kinetic equation for dilute gases is often adopted[3]. Due to the complexity of the collision term in the Boltzmann equation, approximation methods are often used. Among the molecular based methods is the Direct Simulation Monte Carlo method (DSMC). It mimics the Boltzmann equation and is currently the dominant numerical technique for simulating gas flows in transition regime[4]. DSMC has been widely employed for modeling gas flow under non-equilibrium conditions from hypersonic and re-entry vehicle flows to low speed nano-channel flows, and recently to porous media[5-7]. In this method each simulated particle represents a number of real molecules. It is currently the common method for modeling gas flows in the upper rarefaction regime. To obtain accurate results using DSMC there are three constraints regarding time step, cell size and number of particles per cell, which can make the computation expensive.

Several extended hydrodynamic models are developed based on the Boltzmann kinetic equation to simulate rarefied gas flows in the slip and transition regimes[8]. Burnett set of equations are examples of higher order hydrodynamic model[9]. However, these equations suffer from instability problems and they become unstable for small wavelengths and cannot be used for numerical simulations[8,10]. The inappropriateness of the standard NSF model in describing temperature field in a stationary gas in the continuum limit has long been shown by Sone *et al*[11]. Therefore, these authors proved that corrections to the standard constitutive equations involving Korteweg diffuse interface type stress tensor are required to acquire appropriate description of heat transfer processes even in the continuum limit[12].

Brenner first initiated bi-velocity hydrodynamic theory[13]. This consisted of an ad-hoc modification to the Navier-Stokes-Fourier (NSF) constitutive equations. Greenshields and Reese evaluated implications of this modification for the prediction of shock waves thickness and showed that they are better than NSF[14]. The modification was tested for the prediction of mass flow rate in microchannel and it was found to accord well with experimental data[15]. Bi-

velocity hydrodynamic model, which allows as opposed to NSF a form of diffusive mass from the fluid molecular level was later proved to constitute a full thermo-mechanically consistent Burnett regime continuum flow equations[16]. Walls and Abedian used a bi-velocity model to predict the characteristics of a monoatomic Maxwellian gas flow in a micro-channel. Their results indicate that the numerical predictions for the density, temperature, and velocity distributions are different from those previously obtained using original Burnett equations[17].
The lid-driven cavity problem is a fundamental configuration involving a simple geometry. It is often used for validation, benchmarking and testing new methods. Some previous studies showed the complexity involved in a lid-driven cavity flow in rarefied gases under non-equilibrium effects[18]. In the absence of experimental data, results obtained using DSMC are used to compare with extended hydrodynamic equations. Here we used the lid-driven cavity problem to demonstrate how a volume diffusion continuum model can capture non-local-equilibrium phenomena in high Knudsen number heat transfer problems.

VOLUME DIFFUSION MODEL

We consider the following continuum fluid model set of equations that allow for volume diffusion terms in constitutive equations[19].

Conservation of mass

$$\frac{\partial \rho}{\partial t} + \nabla \cdot [\rho \boldsymbol{U}] = 0 \tag{2.1a}$$

Conservation of momentum

$$\frac{\partial \rho \boldsymbol{U}}{\partial t} + \nabla \cdot [\rho \boldsymbol{U}\boldsymbol{U}] + \nabla \cdot [p\boldsymbol{I} + \boldsymbol{\Pi}] = 0 \tag{2.1b}$$

Conservation of total energy

$$\frac{\partial}{\partial t}\left[\frac{1}{2}\rho \boldsymbol{U^2} + \rho e_{in}\right] + \nabla \cdot \left[\frac{1}{2}\rho \boldsymbol{U^2 U} + \rho e_{in}\boldsymbol{U}\right] + \nabla \cdot [(p\boldsymbol{I} + \boldsymbol{\Pi}) \cdot \boldsymbol{U}] + \nabla \cdot \boldsymbol{J_u} = 0 \tag{2.1c}$$

where the shear stress term $\boldsymbol{\Pi}$ is given by**,**

$$\boldsymbol{\Pi} = \boldsymbol{\Pi_v} - \rho \boldsymbol{J_c J_c} \tag{2.2}$$

and

$$\boldsymbol{\Pi_v} = -2\mu \overset{\circ}{\overline{\nabla[\boldsymbol{U} - \boldsymbol{J_c}]}} \tag{2.3}$$

The specific internal energy of the fluid is $e_{in} = (3/2)\,RT$ and p is the pressure. In the above equations the flux $\boldsymbol{J_c}$ is a new molecular level diffusive flux associated with the gas molecule concentration, ρ is the mass density. In other words $-\boldsymbol{J_c}$ is the gas volume diffusive flux. It characterizes macroscopically, the difference between the fluid volume velocity $\boldsymbol{U_v}$ and the fluid mass velocity $\boldsymbol{U}$ [20]:

$$\boldsymbol{J_c} = -\boldsymbol{U_v} + \boldsymbol{U} = -\frac{k_m}{\rho}\nabla\rho \tag{2.4}$$

where k_m is the molecular (or volume) diffusivity coefficient. This coefficient may be related to dynamic viscosity, μ, as:

$$k_m \equiv C_{vv}\frac{\mu}{\rho} \tag{2.5}$$

For our solver it was found convenient to set the dimensionless coefficient as, $C_{vv} = \frac{P_r}{3}$, where P_r is the Prandtl number. The energetic heat flux, $\boldsymbol{J_u}$, is given by,

$$\boldsymbol{J_u} = \boldsymbol{q_{ve}} + p\boldsymbol{J_c} \tag{2.6}$$

where $\boldsymbol{q_{ve}}$ is the entropic heat flux given by the Fourier's law:

$$\boldsymbol{q_{ve}} = -k\nabla T \tag{2.7}$$

In classical NSF theory $\boldsymbol{J_u}$ and $\boldsymbol{q_{ve}}$ are equivalent. Distinction between the energetic heat flux (energy equation) and the entropic heat flux (entropy equation) is a fundamental new aspect of the volume diffusion continuum model. The new energetic heat flux has a component not driven by temperature gradient[21]. The set (2.1) - (2.7) may be viewed as a compressible Korteweg fluid-like set of equations[22]. These equations can be derived by considering a general expression of the fluid local total energy density or entropy using a continuum thermodynamics approach[23].

LID DRIVEN CAVITY PROBLEM

The lid-driven cavity problem considered is shown in Figure 1 and investigated at different Knudsen numbers. The top driven lid (B-C) moves in the *x* direction with a fixed velocity $\mathbf{U_w}$= 100 m/s while all other walls are stationary. All wall temperatures are set to a uniform value of T_w= 273K in all cases. The cavity is of length $W = 10^{-7}m$. A monoatomic argon gas is used. Three different cases are tested with NSF and DSMC[24].

We implemented the set of equations (2.1)-(2.7) with accompanying boundary conditions in the open source package OpenFOAM. In order to find the appropriate number of cells, a grid dependency test was run for 80 x 80, 100 x 100, 160 x 160 and 240 x 240 cells. The mesh containing 160 cells in each direction was selected after the results for ρ and T converged on the mesh of 100 cells. The courant number, C_r was set to 0.5 for all cases as for the continuum methods. For the DSMC method the same cell dependency test was performed for 100 x 100, 200 x 200, 400 x 400. The grid containing 200 x 200 cells is selected for the reported results. The variable hard sphere (VHS) model is used for the DSMC and the collision pairs are chosen based on the no time counter (NTC) method. Fifty particles per cell were initially set for all the cases in order to minimize the statistical noise.

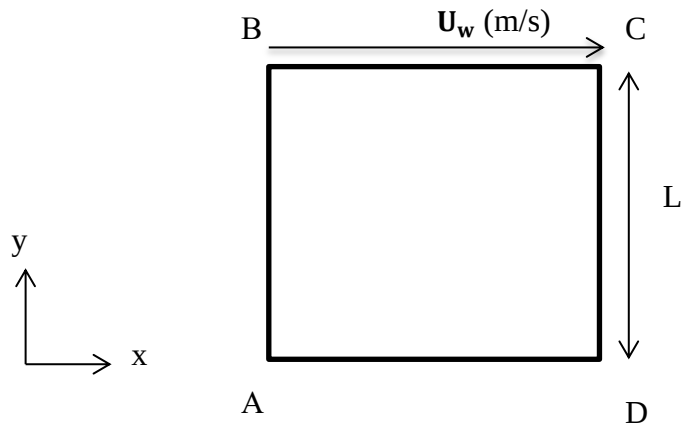

FIG. 1. Configuration of the micro cavity flow problem

Classical NSF is well-known to be unable to capture flow features in transition regime (Kn > 0.1) even when corrected with slip-jump boundary conditions. A lid-driven cavity problem was investigated and compared between DSMC and regularized 13 moments equations (R13)[25]. It was shown that R13 equations describe temperature and heat flux compared to DSMC up to Knudsen number 0.1. The unconventional cold-to-hot heat transfer was observed for Kn > 0.05. Here we run our new solver for three different cases: Kn = 10, Kn = 1 and Kn = 0.1. These are high Knudsen numbers compared with the previous studies[26].

Boundary Conditions

For the two continuum methods, NSF and volume diffusion, a temperature jump boundary conditions were imposed[27]:

$$T - T_w = -\frac{2-\sigma_T}{\sigma_T}\frac{2\gamma}{(\gamma+1)P_r}\lambda\nabla_{\mathbf{n}}T \tag{3.1}$$

$\nabla_{\mathbf{n}} \equiv \mathbf{n}\cdot\nabla$ is the component of the gradient normal to the boundary surface and $\mathbf{n}$ is the unit normal vector defined as positive in the direction of the flow domain. T_w is the wall temperature; γ is the specific heat ratio and σ_T the thermal accommodation coefficient. For all of our simulations the perfect energy accommodation, σ_T=1, was considered. Maxwell slip boundary condition was used for NSF on the velocity[28]:

$$\boldsymbol{U} - \boldsymbol{U_w} = -\left(\frac{2-\sigma_u}{\sigma_u}\right)\frac{\lambda}{\mu}\boldsymbol{\tau} - \frac{3}{4}\frac{\Pr(\gamma-1)}{\gamma p}\mathbf{q} \tag{3.2}$$

where $\mathbf{U_w}$ is the wall velocity, σ_u is the tangential momentum accommodation coefficient and $\boldsymbol{\tau}$ is the tangential shear stress, $\boldsymbol{\tau} = \mathbf{S}\cdot(\mathbf{n}\cdot\boldsymbol{\Pi}_{\mathbf{NSF}})$, where the tensor $\mathbf{S} = \mathbf{I} - \mathbf{nn}$ and $\boldsymbol{\Pi}_{\mathbf{NSF}} = \mu\nabla\boldsymbol{U} + \mu(\nabla\boldsymbol{U})^T - \frac{2}{3}\mathbf{I}\mathrm{tr}(\nabla\boldsymbol{U})$ and $\mathbf{q} = -k\nabla T\cdot\mathbf{S}$

For the volume diffusion continuum model a Maxwell type slip boundary condition is also used but based on the new shear stress tensor and heat flux:

$$\boldsymbol{U} - \boldsymbol{U_w} = -\left(\frac{2-\sigma_u}{\sigma_u}\right)\frac{\lambda}{\mu}\boldsymbol{\tau_v} - \frac{3}{4}\frac{\Pr(\gamma-1)}{\gamma p}\mathbf{j_u} \tag{3.3}$$

where $\boldsymbol{\tau_v}$ is the new tangential shear stress, $\boldsymbol{\tau_v} = \mathbf{S}\cdot(\mathbf{n}\cdot\boldsymbol{\Pi_v})$ and $\mathbf{j_u} = \mathbf{J_u}\cdot\mathbf{S}$. Equation (3.3) implements a new formulation of wall effects within the volume diffusion model. A fully diffuse reflection is adopted for the DSMC simulations.

RESULTS AND DISCUSSION

Numerical results are presented below in the slip and transition flow regimes. For each Knudsen number entropic heat flux and energetic heat flux are depicted and compared with DSMC heat flux.

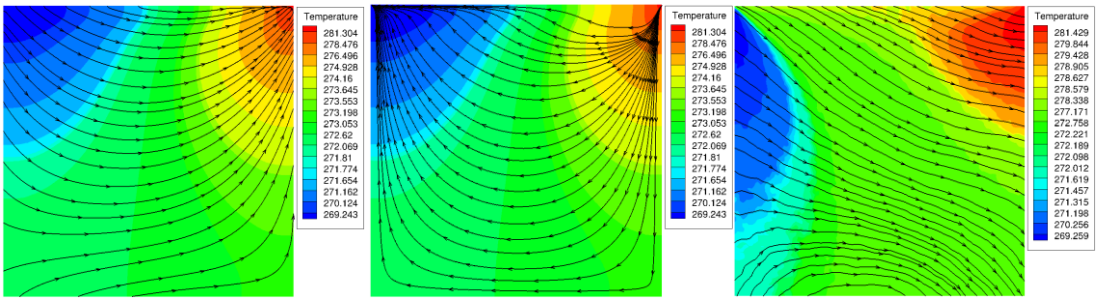

(a) (b) (c)

FIG. 2. Energetic heat flux (*a*) and entropic heat flux (*b*) lines overlaid on the temperature contour for Kn = 10 in comparison with DSMC heat flux (*c*)

Figure 2 compares heat flux lines overlaid the temperature contours. First we observe that the entropic heat flux from the volume diffusion model displays a flow from the higher temperature corner to the lower temperature corner (Figure 2.b), which is in perfect agreement with the Second Law. The phenomenon of cold-to-hot heat transfer

concerns the energetic heat flux (Figure 2.a). While the DSMC heat transfer also shows a heat flux from cold-to-hot, our new model predicts a more consistent energetic heat flux clearly from the left corner to right corner. The unconventional cold-to-hot heat transfer in the energetic heat flux is attributable to the additional term in the heat flux. The predicted temperature distribution is in general agreement with the DSMC. Equal minimum and maximum temperature was predicted from the two methods. The minimum temperature is decreased by four degrees from the initially set conditions, which shows strong non-equilibrium effects in the left corner. The expansion-cooling phenomenon occurring on the left wall shows that the gas temperature becomes lower than the wall temperature ($T_g < T_w$). Another phenomenon governed by viscous dissipation is captured by the volume diffusion model in the right corner (Figure 2.a).

Figure 3 shows the temperature distribution near the top moving lid for the volume diffusion model, DSMC and NSF. Temperature obtained by NSF is constant. This means that NSF does not reveal any disequilibrium for that configuration. This model is therefore inadequate for such a high Knudsen number as expected. Volume diffusion model and DSMC show non-uniform temperature distribution as they capture the non-equilibrium imposed by the moving lid. Volume diffusion model predicts lower temperature near the left wall compared to DSMC. DSMC shows a "plato" in the middle of the cavity while volume diffusion model shows a gradually increasing temperature from left to right. The maximum difference between the two models occurs in the middle of the cavity and is 2.94%. In the mid-transition regime (Figure 4), for Kn = 1, entropic heat flux again follows the Second Law, i.e., a heat transfer from hot-to-cold. The energetic heat flux predicts cold-to-hot heat transfer in agreement with DSMC prediction.

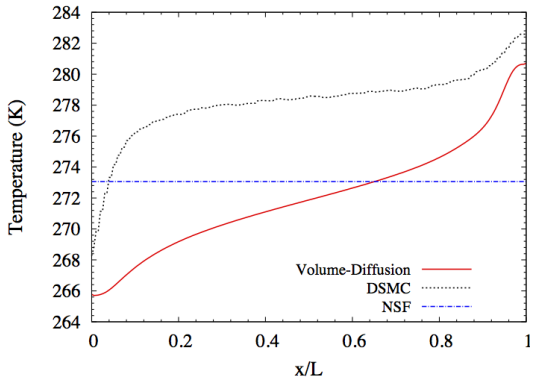

FIG. 3. Variation of gas temperature near the top lid (y/L = 0.9) of the cavity for DSMC, NSF and Volume Diffusion at Kn = 10

The volume diffusion model appears to better predict the energetic cold-to-hot heat transfer phenomenon compared to DSMC. General agreement is observed for the temperature profiles for the two methods. The same maximum temperature is predicted. The similarity between DSMC heat flux and volume diffusion energetic heat flux can be understood. In DSMC, which is a particle based method, heat flux is defined via particle translational kinetic energy.

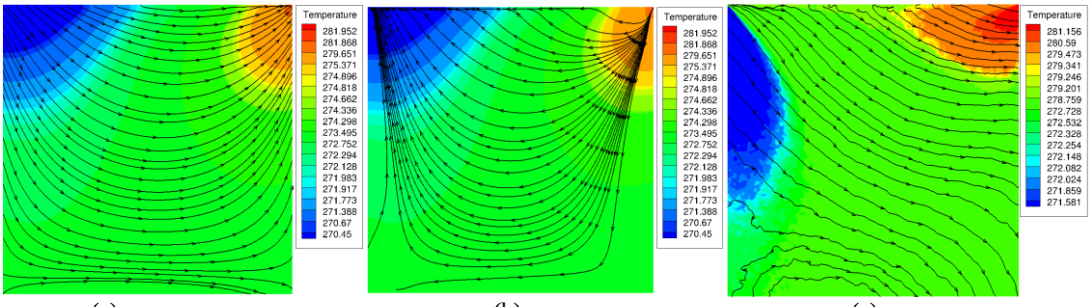

(a) (b) (c)

FIG. 4. Energetic heat flux (*a*) and entropic heat flux (*b*) lines overlaid on the temperature contour for Kn = 1 in comparison with DSMC heat flux (*c*)

At Kn = 1 (Figure 5), NSF is still inadequate in capturing the non-equilibrium imposed by the moving lid as it predicts a constant gas temperature. DSMC and volume diffusion again resolve the non-equilibrium structures with

some minor differences in trend. The maximum relative difference between temperature values from the two methods is about 2.2%. In Figures 3 and 5 the temperature decreases toward the left wall and increases as we approach the right wall for both DSMC and volume diffusion in a Knudsen layer like profile.

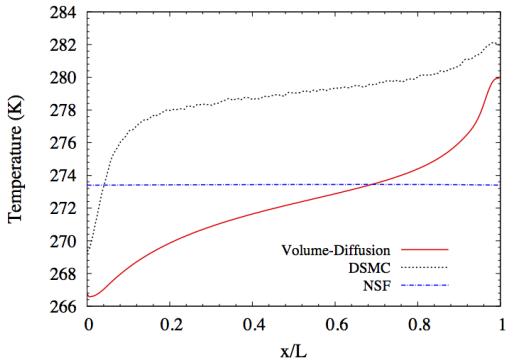

FIG. 5. Variation of gas temperature near the top lid (y/L = 0.9) of the cavity for DSMC, NSF and Volume Diffusion at Kn = 1

As the Knudsen number decreases, the energetic heat flux contour from the volume diffusion model become more similar to DSMC prediction (Figures 6.a vs 6.c). Furthermore, entropic heat flux in Figure 6.b is still consistent with the second law. Both methods predict a low temperature for the lower wall. Agreement is found for the minimum and maximum temperatures.

Comparison of the temperature profile between the three models at Kn = 0.1 is shown in Figure 7. NSF starts to exhibit some non-equilibrium effects at walls. Volume diffusion now predict clear thermal boundary layers at both walls characteristic of Knudsen layers connected with a nearly uniform temperature profile in the middle of the cavity which is close to the NSF value. Overall, NSF prediction is still different from the predictions by DSMC and volume diffusion.

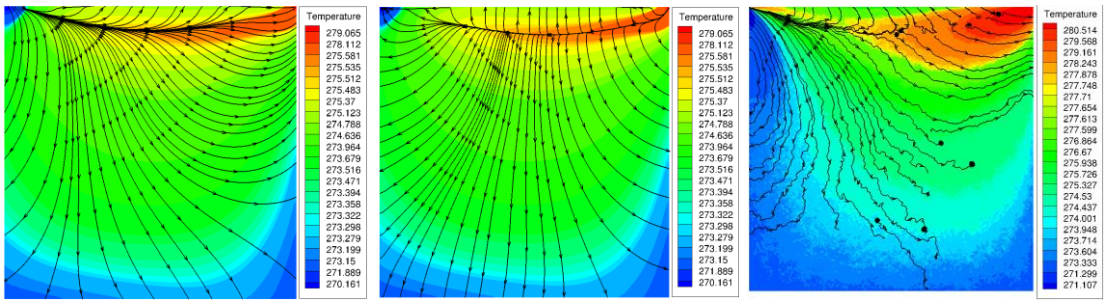

(a) (b) (c)

FIG. 6. Energetic heat flux (*a*) and entropic heat flux (*b*) lines overlaid on the temperature contour for Kn = 0.1 in comparison with DSMC heat flux (*c*)

Agreement is found for the minimum and maximum temperature at the walls between DSMC and volume diffusion. Furthermore, the trends of the two methods are consistent and both methods show that left and right walls are in non-equilibrium state. The average relative difference between temperature values for the DSMC and the volume diffusion is about 2.4%. DSMC shows a temperature shoot near the right wall before converging to the wall temperature. Volume diffusion model has a rather more symmetrical profile.

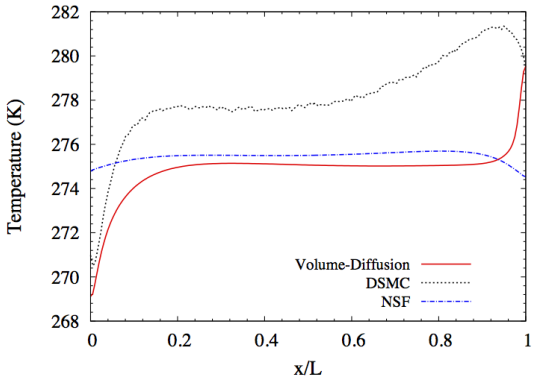

FIG. 7. Variation of gas temperature near the top lid (y/L = 0.9) of the cavity for DSMC, NSF and Volume Diffusion at Kn = 0.1

CONCLUSION

We presented an analysis of non-local-equilibrium heat transfer in rarefied gas flows in a lid-driven cavity using a volume diffusion continuum set of equations. We observed that this continuum model appears to account of non-local equilibrium effects where Navier-Stokes-Fourier fails. Volume diffusion model predicts temperature distribution for the various Knudsen number in general agreement with DSMC for the heat transfer cavity case. While the unconventional cold-to-hot heat transfer is confirmed in high Knudsen numbers, it follows the second law of thermodynamics as the volume diffusion theory distinguishes between entropic heat flux and energetic heat flux. Knudsen layers are well predicted.

REFERENCES:

1. G. Karniadakis, A. Beşkök, and N. R. Aluru, *Microflows and nanoflows : fundamentals and simulation* (Springer, New York, NY, 2005).
2. M. Knudsen, "Die Gesetze der Molekularströmung und der inneren Reibungsströmung der Gase durch Röhren," Annalen der Physik **333**, 75 (1909).
3. C. Cercignani, *Theory and application of the Boltzmann equation* (Scottish Academic Press, 1975).
4. G. A. Bird, *Molecular gas dynamics and the direct simulation of gas flows* (Oxford University Press, Oxford, 1994).
5. C. White, M. K. Borg, T. J. Scanlon, and J. M. Reese, "A DSMC investigation of gas flows in micro-channels with bends," Computers & Fluids **71**, 261 (2013).
6. N. T. P. Le, A. Shoja-Sani, and E. Roohi, "Rarefied gas flow simulations of NACA 0012 airfoil and sharp 25–55-deg biconic subject to high order nonequilibrium boundary conditions in CFD," Aerospace Science and Technology **41**, 274 (2015).
7. C. Christou, and S. K. Dadzie, "Direct-Simulation Monte Carlo Investigation of a Berea Porous Structure," SPE Journal (2015).
8. L. S. García-Colín, R. M. Velasco, and F. J. Uribe, "Beyond the Navier–Stokes equations: Burnett hydrodynamics," Physics Reports **465**, 149 (2008).
9. D. Burnett, "The distribution of velocities in a slightly non-uniform gas," Proceedings of the London Mathematical Society **2**, 385 (1935).
10. H. Struchtrup, and M. Torrilhon, "Regularization of Grad's 13 moment equations: derivation and linear analysis," Physics of Fluids (1994-present) **15**, 2668 (2003).
11. Y. Sone, K. Aoki, S. Takata, H. Sugimoto, and A. Bobylev, "Inappropriateness of the heat- conduction equation for description of a temperature field of a stationary gas in the continuum limit: Examination by asymptotic analysis and numerical computation of the Boltzmann equation," Physics of Fluids (1994-present) **8**, 628 (1996).
12. Y. Sone, "Flows induced by temperature fields in a rarefied gas and their ghost effect on the behavior of a gas in the continuum limit," Annual review of fluid mechanics **32**, 779 (2000).
13. H. Brenner, "Kinematics of volume transport," Physica A: Statistical Mechanics and its Applications **349**, 11 (2005).

14. C. J. Greenshields, and J. M. Reese, "The structure of shock waves as a test of Brenner's modifications to the Navier–Stokes equations," Journal of Fluid Mechanics **580**, 407 (2007).
15. S. K. Dadzie, and H. Brenner, "Predicting enhanced mass flow rates in gas microchannels using nonkinetic models," Physical Review E **86**, 036318 (2012).
16. S. K. Dadzie, "A thermo-mechanically consistent Burnett regime continuum flow equation without Chapman–Enskog expansion," Journal of Fluid Mechanics **716**, R6 (2013).
17. P. L. Walls, and B. Abedian, "Bivelocity gas dynamics of micro-channel couette flow," International Journal of Engineering Science **79**, 21 (2014).
18. B. John, X.-J. Gu, and D. R. Emerson, "Effects of incomplete surface accommodation on non-equilibrium heat transfer in cavity flow: A parallel DSMC study," Computers & Fluids **45**, 197 (2011).
19. S. K. Dadzie, and J. M. Reese, "A volume-based hydrodynamic approach to sound wave propagation in a monatomic gas," Physics of Fluids (1994-present) **22**, 016103 (2010).
20. S. K. Dadzie, J. M. Reese, and C. R. McInnes, "A continuum model of gas flows with localized density variations," Physica A: Statistical Mechanics and its Applications **387**, 6079 (2008).
21. H. Brenner, "Beyond Navier–Stokes," International Journal of Engineering Science **54**, 67 (2012).
22. M. Heida, and J. Málek, "On compressible Korteweg fluid-like materials," International Journal of Engineering Science **48**, 1313 (2010).
23. D. M. Anderson, G. B. McFadden, and A. A. Wheeler, "Diffuse-interface methods in fluid mechanics," Annual review of fluid mechanics **30**, 139 (1998).
24. T. Scanlon, C. White, M. K. Borg, R. C. Palharini, E. Farbar, I. D. Boyd, J. Reese, and R. Brown, "Open souce DSMC chemistry modelling for hypersonic flows," AIAA Journal (2014).
25. A. Mohammadzadeh, E. Roohi, H. Niazmand, S. Stefanov, and R. S. Myong, "Thermal and second-law analysis of a micro- or nanocavity using Direct-Simulation Monte Carlo," Physical review. E, Statistical, nonlinear, and soft matter physics **85**, 056310 (2012).
26. B. John, X.-J. Gu, and D. R. Emerson, "Investigation of Heat and Mass Transfer in a Lid-Driven Cavity Under Nonequilibrium Flow Conditions," Numerical Heat Transfer, Part B: Fundamentals **58**, 287 (2010).
27. M. Smoluchowski von Smolan, "Über wärmeleitung in verdünnten gasen," Annalen der Physik **300**, 101 (1898).
28. J. C. Maxwell, "On Stresses in Rarefied Gases Arising from Inequalities of Temperature," Proceedings of the Royal Society of London **27**, 304 (1878).